Book Chapter

Thermogravimetric Analysis and Kinetic Modeling of Nanche Stone BSC Pyrolysis: A Potential Agro-Industrial Waste for Bioenergy Production

Jonathan M Sanchez-Silva[1], Raúl Ocampo-Pérez[1], Erika Padilla-Ortega[1], Diakaridia Sangaré[2], Miguel A Escobedo-Bretado[3], Jorge L Domínguez-Arvizu[4], Blanca C Hernández-Majalca[4], Javier E Morales-Mendoza[4], Alejandro López-Ortiz[4]* and Virginia Collins-Martínez[4]

[1]Centro de Investigación y Estudios de Posgrado, Facultad de Ciencias Químicas, Universidad Autónoma de San Luis Potosí, Mexico
[2]Institut Universitaire de Technologie, Université d'Orléans, France
[3]Facultad de Ciencias Químicas, Universidad Juárez del Estado de Durango, Mexico
[4]Centro de Investigación en Materiales Avanzados, Departamento de Ingeniería y Química de Materiales, Mexico

***Corresponding Author:** Alejandro López-Ortiz, Centro de Investigación en Materiales Avanzados, Departamento de Ingeniería y Química de Materiales, S.C., Miguel de Cervantes 120, Chihuahua 31136, Mexico

Published **May 23, 2023**

This Book Chapter is an excerpt of an article published by Alejandro López-Ortiz, et al. at Molecules in January 2023. (Sanchez-Silva, J.M.; Ocampo-Pérez, R.; Padilla-Ortega, E.; Sangaré, D.; Escobedo-Bretado, M.A.; Domínguez-Arvizu, J.L.; Hernández-Majalca, B.C.; Salinas-Gutiérrez, J.M.; López-Ortiz, A.; Collins-Martínez, V. Pyrolysis Kinetics of Byrsonima crassifolia Stone as Agro-Industrial Waste through Isoconversional Models. Molecules 2023, 28, 544. https://doi.org/10.3390/molecules28020544)

How to cite this book chapter: Jonathan M Sanchez-Silva, Raúl Ocampo-Pérez, Erika Padilla-Ortega, Diakaridia Sangaré, Miguel A Escobedo-Bretado, Jorge L Domínguez-Arvizu, Blanca C Hernández-Majalca, Javier E Morales-Mendoza, Alejandro López-Ortiz, Virginia Collins-Martínez. Thermogravimetric Analysis and Kinetic Modeling of Nanche Stone BSC Pyrolysis: A Potential Agro-Industrial Waste for Bioenergy Production. In: Prime Archives in Molecular Sciences: 4th Edition. Hyderabad, India: Vide Leaf. 2023.

Abstract

The aim of this study is to examine the pyrolysis kinetics of Nanche stone BSC (Byrsonima crassifolia), a type of agro-industrial waste, through non-isothermal thermogravimetric experiments. By identifying the triplet kinetics (including apparent activation energy, pre-exponential factor, and reaction model) and thermodynamic parameters, we intend to collect essential information for the design, construction, and operation of a pilot-scale reactor to pyrolyze this lignocellulosic residue. The findings suggest that BCS has low levels of moisture and ash, while exhibiting a high percentage of volatile matter (≥70%). These characteristics make BCS a promising candidate for producing a range of bioenergy products. Average apparent activation energies obtained from different methods (KAS, FWO and SK) were consistent in value (~123.8 kJ/mol). The pre-exponential factor from the Kissinger method ranged from 10^5 to 10^{14} min^{-1} for the highest pyrolytic activity stage, indicating a high-temperature reactive system The thermodynamic analysis showed that the difference between E_A and ΔH is small (5.2 kJ/mol), which is favorable for the pyrolysis reaction and indicates that the energy process is feasible. The analysis of the reaction models, using the master plot method, revealed that the pyrolytic degradation is primarily governed by a decreasing

reaction order with respect to the degree of conversion. Furthermore, BCS exhibits a relatively high calorific value of 14.9 MJ/kg, coupled with a comparatively low average apparent activation energy of 122.7 kJ/mol as determined by the Starink method. These characteristics show BCS highly suitable for utilization in value-added energy production.

Keywords

Pyrolysis Kinetic Triplet; *Byrsonima crassifolia*; Lignocellulosic Biomass; Isoconversional Methods; Thermodynamic Analysis

Introduction

The most pressing environmental issue facing the world today is undoubtedly climate change, which has negative impacts on the economy and the energy sector. The root cause of this phenomenon is primarily environmental pollution and the greenhouse gas emissions resulting from the overuse of fossil fuels. Therefore, there is an urgent need to explore and develop alternative energy sources [1].

Biomass has emerged as a significant renewable energy source and is now considered the fourth most relevant energy source worldwide after coal, oil, and natural gas [2]. Lignocellulosic residues derived from various agro-industrial sectors are a sustainable and viable option for generating energy due to their abundance, low cost, low greenhouse gas emissions, and carbon neutrality [3,4]. These residues comprise of three primary components, namely hemicellulose (20–40%), cellulose (40–60%), and lignin (10–25%) [5], making them favorable for conversion into liquid, solid, and gaseous products through different conversion processes, such as biochemical, thermochemical, and physicochemical methods [6].

Nanche, scientifically known as *Byrsonima crassifolia*, is a tropical and subtropical fruit species that is found in Mexico, Central, and South America [7]. The fruit, which is a yellow-orange drupe, is harvested from July to September and has a fibrous pulp that surrounds a hard and woody endocarp,

commonly referred to as the "stone" [8]. The consumption of this fruit has recently increased due to its high content of antioxidants and unsaturated fatty acids [9,10]. In Mexico, 9262 tons of fruit were produced in 2020, with a planted area of 1752 hectares [11]. As the endocarp comprises between 25-34% of the total fruit weight [12], it is considered a significant agro-industrial waste with the potential to be converted through various thermochemical processes, such as liquefaction, combustion, hydrothermal carbonization, gasification, or pyrolysis. These processes enable the conversion of the primary biomass components into valuable energy products [13].

Thermochemical processes provide an opportunity to utilize agro-industrial wastes to produce gaseous, liquid, and solid fuels [14]. Pyrolysis is one such process that is renewable, cost-effective, and efficient for converting agro-industrial wastes [15]. However, there is a significant challenge in understanding the factors that influence the process, especially for designing, scaling up, and operating pyrolysis reactors. Pyrolysis is the thermal degradation of organic matter without oxygen, leading to the production of biochar, bio-oil, tar (an aqueous solution of organic compounds), and gaseous products [16]. The process occurs at temperatures ranging from 300 to 600°C in an inert atmosphere to prevent combustion and gasification reactions. It is noteworthy that the products obtained from pyrolysis are more valuable than the raw material [14].

The thermal degradation behavior of biomass, fuels, and other compounds is commonly examined through thermogravimetric analysis (TGA) and differential thermal analysis (DTG) techniques. These methods provide valuable data on the thermal behavior and kinetics of the material under different heating rates. TGA and DTG are widely used for the evaluation of characteristics and degradation kinetics of biomass due to their accuracy and simplicity [16,17]. These analyses can also provide important information on the kinetic triplet of the process, including the apparent activation energy (E_A), pre-exponential factor (A_α), and reaction mechanism or kinetic model, $f(\alpha)$ [6,18]. By estimating these parameters, it is possible to evaluate the thermodynamic properties of the pyrolysis process, including

the ΔH, ΔG, and ΔS values. These parameters are critical for evaluating the energetic feasibility of the pyrolysis process [13,18].

In the literature, there are several studies of biomass pyrolysis using various agro-industrial wastes such as avocado stone, *Agave salmiana* bagasse, and cocoa shell by Sangaré et al. [18], apple pomace by Baray-Guerrero et al. [19], garlic husk by Singh et al. [20], peanut shells by Açıkalın [17], corn stalk by Cai et al. [15], wheat straw by Mani et al. [21], and waste sawdust by Mishra & Mohanty [5], using various kinetic methods. However, the reported results are different for each agro-industrial waste due to different physicochemical characteristics and pyrolytic operating conditions [22]. The kinetic analysis of biomass thermal degradation is generally based on the degradation rate equation developed by Friedman in 1964 [23], and the ICTAC (International Confederation for Thermal Analysis and Calorimetry) committee has evaluated integral isoconversional methods such as Kissinger–Akahira–Sunose (KAS), Flynn–Wall–Ozawa (FWO), and Starink (SK), and concluded that the SK method is the most valid and reliable integral isoconversional method for the estimation of apparent kinetics [24]. This method can provide effective and accurate activation energies for kinetic analysis of biomass pyrolysis [1,15,24]. Therefore, the physicochemical characterization composed of the proximal and compositional analysis of biomass, the kinetic study involving the kinetic triplet in combination with the calculation of the thermodynamic parameters; enthalpy (ΔH), Gibbs free energy (ΔG), and entropy (ΔS) of the pyrolysis process, represent a set of information that is fundamental for the design, construction, and operation of a large-scale reactor for the pyrolysis of any lignocellulosic residue [16].

The aim of this study is to investigate the pyrolysis kinetics of Nanche (*Byrsonima crassifolia*) stone, a biomass waste, for the first time. This will be achieved by conducting a physicochemical characterization of the waste and analyzing the kinetic triplet, which consists of the apparent activation energy, pre-exponential factor, and reaction model. In addition, the

thermodynamic parameters, namely enthalpy (ΔH), Gibbs free energy (ΔG), and entropy (ΔS), will be estimated. The findings of this research will provide insight into the potential use of Nanche stone as a valuable bioenergy resource.

Materials and Methods

Feedstock Preparation and Characterization

The Nanche (*Byrsonima crassifolia*, BCS) endocarp was collected in the state of Nayarit, México and was dried (100 °C for 24 hr), crushed, and sieved to particle sizes using standard sieves according to ASTM E11 procedure as follows: $75 < Dp_1 < 150$ µm, $150 < Dp_2 < 300$ µm, $600 < Dp_3 < 850$ µm and $850 < Dp_4 < 1680$ µm, which correspond to Mesh Numbers of 200, 100, 30, and 20, respectively. Biomass characterization consisted of evaluating the following: (i) Elemental analysis and ash content using an elemental analyzer (Carlo Erba Ea-1110) coupled to ICP (Thermo Jarrell Ash IRIS/AP DUO ICP), (ii) Calorific value using an adiabatic bomb calorimeter (Parr-1341 Oxygen Bomb Calorimeter) following the ASTM D-2015-96 standard method, (iii) Lignin, cellulose, and hemicellulose content by gravimetric techniques described in ASTM (E1756-95, D1106-95, and D1103-60), and (iv) Moisture, volatiles, and ash content according to the procedure described in ASTM E (871-82), ASTM (872-82), and ASTM (1755-1795), respectively.

Thermogravimetric Analysis

The thermal degradation of the Nanche endocarp was investigated using a thermogravimetric analyzer (TA Instruments, Q500). Thermogravimetric analysis (TGA) data were collected in a temperature range between 30 and 900 °C to completely evaluate the deconvolution of DTG considering the region of decomposition of hemicellulose, cellulose, and lignin. According to the ICTAC recommendations [24–26], it is required to use slow heating rates to avoid self-heating/cooling and to generally minimize the adverse heat and mass transfer phenomena, for which the following heating rates (β) were chosen: 5, 10, and 15 °C/min under a nitrogen atmosphere (N_2,

flow rate: 100 cm^3/min) and using a BCS mass of ~30 mg. The differential thermogravimetric analysis (DTG) was calculated using Origin Plot Software from the different data generated by the decomposition heating rates previously performed. To find the appropriate particle size (D_p) for the kinetic analysis, samples with different particle sizes were analyzed: 200, 100, 30, and 20 mesh at 5 °C/min.

Kinetic Triplet Estimation

The process of thermochemical conversion of biomass is highly intricate, involving the simultaneous degradation of hemicellulose, cellulose, and lignin, and their subsequent interactions with degradation products [19,27]. To simplify the kinetic analysis, the overall biomass pyrolysis reaction is usually represented by the following general reaction scheme:

$$Lignocellulosic\ biomass \xrightarrow{k(T)} Vollatiles + biochar$$

The general expression for biomass pyrolysis kinetics is evaluated by the degradation rate, which is a function of temperature (T) and degree of conversion (α) and can be expressed by Equation (1).

$$\frac{d\alpha}{dt} = k(T) * f(\alpha) \quad (1)$$

where k corresponds to the apparent rate constant, f(α) is the model-based function of conversion, and α is the degree of conversion which is expressed as:

$$\alpha = \frac{(m_o - m_t)}{(m_o - m_\infty)} \quad (2)$$

where m_o is the initial weight of biomass sample, m_t is its weight at time t, and m_∞ is the weight of char at the end of the thermal degradation. Incorporating the Arrhenius type equation, Equation (1) converts to:

$$\frac{d\alpha}{dt} = A\ exp\left(\frac{-E_A}{RT}\right) f(\alpha) \quad (3)$$

Here, E_A is the apparent activation energy (kJ/mol), A is the pre-exponential factor (min^{-1}), T is the temperature (K), and R is the universal gas constant (8.314 J/K mol). During pyrolysis, the temperature increases with time since a heating rate in an inert atmosphere is fixed (β, °C/min), which can also be expressed as follows using the chain rule:

$$\frac{d\alpha}{dT} = \frac{A}{\beta}\ exp\left(\frac{-E_A}{RT}\right)\ f(\alpha) \tag{4}$$

Combining Equations (3) and (4), results:

Equation (5) refers to the biomass degradation during pyrolysis and is used to calculate the kinetic parameters involved in the process. The integration as a function of temperature of Equation (5) gives the following results:

$$\beta = \frac{dT}{dt} = \frac{dT}{d\alpha} * \frac{d\alpha}{dt} \tag{5}$$

The integral form of Equation (6) is obtained by solving the integral as follows:

$$g(\alpha) = \int_0^{\alpha} \frac{d\alpha}{f(\alpha)} = \frac{A}{\beta}\int_{T_o}^{T} exp\left(\frac{-E_A}{RT}\right) dT \tag{6}$$

where g(α) is the integrated reaction model, x is equal to E_A/RT, p(x) is the exponential integral of temperature and has no analytical solution. Generally, Equations (6) and (7) are used to determine the kinetic triplet; apparent activation energy, pre-exponential factor, and reaction model [22].

$$g(\alpha) = \frac{AE_A}{\beta R}\int_0^{\infty} exp(-u)du = \frac{A\,E_A}{\beta\,R}p(x) \tag{7}$$

Estimation of Apparent Activation Energy (E_A)

Various mathematical models have been proposed to solve Equation (6) in isoconversional methods [5,28]. In this study, we evaluated the kinetic triplet by estimating the apparent activation energy (EA) using integral isoconversional models such as

Kissinger–Akahira–Sunose (KAS), Flynn–Wall–Ozawa (FWO), and Starink (SK). These models are presented below:

Kissinger–Akahira–Sunose (KAS) method is an integral isoconversional method that was first proposed by Kissinger [29] and later modified by Akahira and Sunose [30]. The KAS method employs a simple approximation for the exponential integral, $px = x^{-2}e^{x}$. By introducing this approximation in Equation (6), the following expression is obtained:

$$ln\left(\frac{\beta_i}{T_{\alpha,i}{}^2}\right) = ln\left(\frac{A_\alpha R}{E_A g(\alpha)}\right) - \frac{E_A}{RT_{\alpha,i}} \quad (8)$$

For each degree of conversion, the $ln\left(\frac{\beta_i}{T_{\alpha,i}{}^2}\right)$ vs. $\frac{1}{T_{\alpha,i}}$ is plotted using the experimental data, and from the slope of the straight lines, the apparent activation energy is obtained.

$$ln\,(\beta_i) = ln\left(\frac{A_\alpha E_A}{g(\alpha)R}\right) - 5.331 - 1.052\frac{E_A}{RT_{\alpha,i}} \quad (9)$$

The *Flynn–Wall–Ozawa (FWO)* method is another integrated isoconversional technique for calculating the apparent activation energy. The FWO method was proposed by Ozawa [31] and Flynn and Wall [32] and it uses Doyle's linear approximation instead of the temperature integral for Equation (6): $\ln P(x) \approx$

$-5.331 - 1 - 052x$. The FWO method can be expressed as follows:

The apparent activation energy can be calculated through the slope of the plot between $ln(\beta_i)$ vs. $1/T_{\alpha,i}$

The *Starink (SK)* method is another integral isoconversional technique that has been widely used to calculate the apparent activation energy [33,34]. This method is based on a modified form of the Kissinger equation, considering the temperature dependence of the pre-exponential factor. The SK method is expressed as follows:

$$ln\left(\frac{\beta_i}{T_{\alpha,i}{}^{1.92}}\right) = Constant - 1.0008\frac{E_A}{RT_{\alpha,i}} \quad (10)$$

Here, $ln\left(\frac{\beta_i}{T_{\alpha,i}{}^{1.92}}\right)$ versus $\frac{1}{T_{\alpha,i}}$ is plotted to obtain a set of straight lines at different conversions, where the apparent activation energy can be obtained from the slopes of these lines.

Estimation of the Pre-Exponential Factor (A_α)

Although the isoconversional methods mentioned above are useful in determining the apparent activation energy, the calculated value of A_α using these methods is often deemed unreliable [35]. Thus, the ASTM E698-18 standard method, based on Kissinger's equation, is employed, as it provides a more accurate estimate of the activation energy. The equation is presented below:

$$ln\left(\frac{\beta}{T_p{}^2}\right) = ln\left(\frac{A_\alpha R}{E_A g(\alpha)}\right) - \frac{E_A}{RT_p} \quad (11)$$

In this method, the temperature at the maximum peak of the DTG plot for a given value of β is denoted by Tp. The value of E_A is then calculated using the isoconversional methods described above, for different conversion levels α. Once the values of E_A are known, Equation (12) is derived from Equation (11) to calculate A_α [6,35].

$$A_\alpha = \frac{\beta E_{A,\alpha_i} exp\left(\frac{E_{A,\alpha_i}}{RT_p}\right)}{RT_p{}^2} \quad (12)$$

Estimation of the Reaction Model

Various kinetic methods have been reported in the literature, and several reaction models have been proposed to describe the overall solid-state reaction [20,22]. One such method is the master plots method [28,36], which employs the Taylor series approach to estimate the exponential temperature integral and can be mathematically expressed as follows:

$$g(\alpha) = \frac{AE_A}{\beta R} p(x) = \frac{AE_A}{\beta R}\left[\frac{e^{-x}}{x^2}\left(1 - \frac{2!}{x} + \frac{3!}{x^2} + \frac{4!}{x^3} + \cdots\right)\right] \quad (13)$$

For $20 \leq x \leq 50$ and using the normalized equation [Equation (14)], masters plots are developed, considering the integral models described in Table 1, and by plotting the experimental and model data in parallel, the reaction model associated with the thermal degradation of biomass can be defined [5].

$$\lambda(\alpha) = \frac{g(\alpha)_i}{g(\alpha)_{0.5}} = \frac{p(x)_i}{p(x)_{0.5}} \quad (14)$$

where g(α)0.5 is the integral model at α = 0.5 and p(x)0.5 is the approximation for α = 0.5, where $x = E_{A,\alpha:0.5}/RT_{\alpha:0.5}$. The main reaction model is chosen by comparing the theoretical and experimental curves, where the theoretical curve with the

$$SS_E = \sum_{i=1}^{N} \left(\lambda(\alpha)_{exp} - \lambda(\alpha)_{calc}\right)^2 \quad (15)$$

smallest value of sums square error (SSE, Equation (15)) is selected as the reaction model [20].

where N is the number of data points; λ(α)exp is the experimental master plot equation; λ(α)calc is the calculated master plot normalized equation by the integral models.

Table 1: Expressions for f(α) and g(α) functions of reaction models to describe thermal decomposition solid state reactions (Sangaré et al. and Mumbach et al.) [18,19].

Reaction model		*f(α)*	*g(α)*
Reaction order models			
R1	Mampel (first order)	1 - α	-ln(1 - α)
R2	Second order	$(1 - \alpha)^2$	$(1 - \alpha)^{-1} - 1$
R3	Third order	$(1 - \alpha)^3$	$0.5[(1 - \alpha)^{-2} - 1]$
R4	One and half order	$(1 - \alpha)^{3/2}$	$[(1 - \alpha)^{-1/2} - 1]$
Rn	n-order reaction	$(1 - \alpha)^n$	$[1-(1 - \alpha)^{1-n}]/(1-n)$
Diffusion models			

D1	One dimensional	$0.5\ \alpha^{-1}$	α^2
D2	Two dimensional (Valensi model)	$[-\ln(1-\alpha)]^{-1}$	$(1-\alpha)\ln(1-\alpha)+\alpha$
D3	Diffusion control (Jander control)	$(1-\alpha)^{2/3}[1-(1-\alpha)^{1/3}]^{-1}$	$[1-(1-\alpha)^{1/3}]^2$
D4	Diffusion control (Ginstling model)	$(3/2)[(1-\alpha)^{-1/3}-1]^{-1}$	$1-(2/3)\alpha-(1-\alpha)^{2/3}$
Power law nucleation models			
P1	Power law	$(2/3)\alpha^{-1/2}$	$\alpha^{3/2}$
P2	Power law	$2\alpha^{1/2}$	$\alpha^{1/2}$
P3	Power law	$3\alpha^{2/3}$	$\alpha^{1/3}$
P4	Power law	$4\alpha^{3/4}$	$\alpha^{1/4}$
Random nucleation and subsequent growth models			
A1	Avarami-Erofeev	$1.5(1-\alpha)[-\ln(1-\alpha)]^{1/3}$	$[-\ln(1-\alpha)]^{2/3}$
A2	Avarami-Erofeev	$2(1-\alpha)[-\ln(1-\alpha)]^{1/2}$	$[-\ln(1-\alpha)]^{1/2}$
A3	Avarami-Erofeev	$3(1-\alpha)[-\ln(1-\alpha)]^{2/3}$	$[-\ln(1-\alpha)]^{1/3}$
A4	Avarami-Erofeev	$4(1-\alpha)[-\ln(1-\alpha)]^{3/4}$	$[-\ln(1-\alpha)]^{1/4}$
A5	Random nucleation	$(1-\alpha)^2$	$(1-\alpha)^{-1}$
A6	Random nucleation	$0.5(1-\alpha)^3$	$(1-\alpha)^{-2}$
Geometrical contraction models			
F2	Contracting cylinder	$2(1-\alpha)^{1/3}$	$1-(1-\alpha)^{1/2}$
F3	Contracting sphere	$2(1-\alpha)^{2/3}$	$1-(1-\alpha)^{1/3}$

Estimation of Thermodynamic Parameters

Thermodynamic properties, such as Gibbs free energy (ΔG), enthalpy (ΔH), and entropy (ΔS), are essential for evaluating the feasibility of a thermochemical conversion process in terms of energy requirements [13]. These properties can be estimated

using the apparent activation energy and the pre-exponential factor determined by the methods described above [6]. The thermodynamic parameters can be calculated using the following equations:

$$\Delta G = E_A + RT_p \, ln\left(\frac{k_B \, T_p}{h \, A_\alpha}\right) \quad (16)$$

$$\Delta H = E_A + RT_p \quad (17)$$

$$\Delta S = \frac{\Delta H - \Delta G}{T_p} \quad (18)$$

Here k_B is the Boltzmann constant (1.381×10^{-23} J/K, h is the Plank constant 6.626×10^{-34} J/s. All kinetic triplet calculations and thermodynamic parameters were determined using Microsoft Excel.

Results and Discussions

Biomass Physicochemical Characterization

Table 2 presents the results of the characterization of the Nanche stone. From these results, it is evident that there is a low ash content (2.2 wt %), a high volatile content (71.7 wt %), and a significant amount of fixed carbon (14.8 wt %), which is characteristic of lignocellulosic biomasses, making this residual biomass attractive for thermal degradation processes and biochar generation [27]. Regarding the mineral composition of the ash, the highest contributions come from alkali metals such as potassium (76.38 wt %), sodium (7.95 wt %), and calcium (6.66 wt %), this high composition is beneficial for the thermochemical conversion process. It has been shown that these metals could modify the crystalline structure of cellulose and further promote reactivity during pyrolysis [36]. The elemental analysis shows that the Nanche stone has a small amount of N (1.52 wt %) and no S, which is advantageous because it minimizes corrosion problems associated with the formation of acids in thermochemical processing equipment. It is also evident that the highest elemental amount corresponds to carbon, with 49.88 wt %, followed by oxygen, with 42.95 wt %. From the

lignocellulosic composition, it is important to note the high content of cellulose (44.16 wt %) and lignin (34.67 wt %), which gives high rigidity and hardness to the biomass. Finally, the calorific power value (14.93 MJ/kg) is among values commonly found in different biomasses such as Rice husk (17.96 MJ/kg), Wheat Straw (15.29 MJ/kg), Sugar cane bagasse (18.56 MJ/kg), Banana trunk (13.41 MJ/kg), and Rice Straw (15.06 MJ/kg) [28], where biomass having higher volatile matter content and low moisture content presents high calorific power value and better ignition and combustion rate [5].

Table 2: Characterization of BCS.

Elemental analysis (wt %, dry basis)	
C	49.88
H	5.65
N	1.52
O [a]	42.95
S	N.D.
Compositional analysis (wt %, dry removable-free basis)	
Cellulose [a]	44.16
Hemicellulose	21.17
Lignin	34.67
Extractibles with ethanol	2.01
Proximate analysis (wt %, dry basis)	
MC	11.3
VM	71.7
FC [a]	14.8
Ash	2.2
Ash composition (wt %)	
B	0.23
Ba	0.42
Ca	6.66
Co	0.02
Cr	0.21
Cu	0.34
Fe	1.41
K	76.38
Mg	1.59
Mn	0.61
Mo	0.03
Na	7.95
Ni	0.26
Si	2.49

Sr	0.83
Ti	0.16
Zn	0.40
Physical properties (dry basis)	
Bulk density (kg/m^3)	980
Calorific Power (MJ/kg)	14.93

MC: moisture content; VM: volatile matter; FC: fixed carbon; [a]; by difference; N.D: non detected.

Thermogravimetric Analysis (TGA & DTG)

Particle Size Effect

Figure 1 shows the TGA and DTG curves obtained from experimental data and calculations for the Nanche endocarp, considering a heating rate of 5 °C/min and varying particle sizes. In Figure 1, it is evident that the devolatilization phase takes place within the temperature range of 250 °C to 450 °C. Notably, when the particle size is reduced to Dp < 600 µm, a more pronounced devolatilization of the biomass occurs, accounting for approximately 79% of the total mass loss. This enhanced devolatilization leads to an augmented production of volatile materials while concurrently decreasing the production of biochar. Refer to Figure 1 for a visual representation of these trends [37].

The DTG curves, depicted in Figure 1, exhibit distinct patterns associated with hemicellulose degradation. Notably, a clear shoulder is observed around 275 °C, indicating changes in the degradation behavior of hemicellulose. This phenomenon can be attributed to a clogging effect caused by cross-linked hemicellulose present in the lignin structure.

Furthermore, the particle size of the biomass plays a crucial role in these degradation processes. Smaller particle sizes offer a larger exposed surface area, facilitating the more efficient release of decomposed hemicellulose into the inert atmosphere. This effect is visually evident in the DTG curves, where a decrease in particle size leads to a more pronounced and distinct peak related to hemicellulose degradation.

Additionally, the DTG curves also highlight that larger particle sizes contribute to a shift in the temperature of the maximum peak, indicating variations in the kinetics of the reactions involved. Moreover, there is a noticeable discrepancy in the decline of the cellulose degradation peak within the temperature range of 340–367 °C, further emphasizing the influence of particle size on the degradation behavior of cellulose. For a comprehensive visualization of these findings, refer to Figure 1. These variations may be attributed to heat and mass transfer problems [38].

To examine the impact of heating rate, we specifically chose a particle size range (850 μm < Dp4 < 1680 μm, mesh #20) that demonstrated the most consistent behavior. Among the tested particle sizes, this range exhibited distinct and well-defined peaks corresponding to hemicellulose, cellulose, and lignin on the DTG curve, making it highly suitable for a comprehensive analysis employing the deconvolution technique outlined below. This selected particle size range allows for a thorough investigation of the thermal decomposition process, as it provides clear and distinguishable peaks associated with the individual components of the biomass. By employing the deconvolution technique, the contributions of hemicellulose, cellulose, and lignin to the overall decomposition profile can be accurately assessed, enabling a comprehensive understanding of the thermal behavior of the biomass. The DTG curve for this particle size range serves as an excellent basis for a complete analysis, providing valuable insights into the thermal decomposition process.

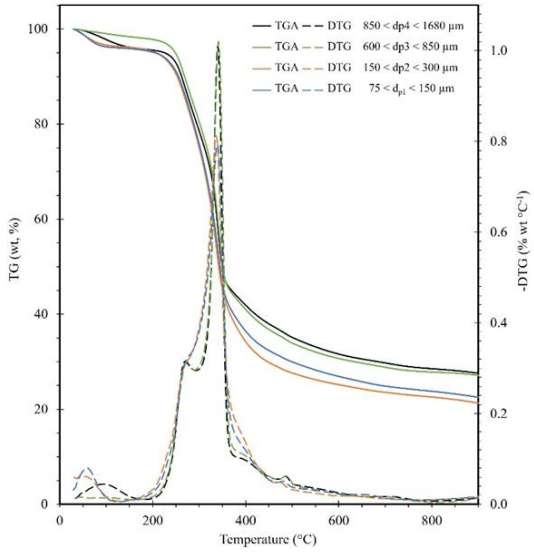

Figure 1: TGA and DTG curves for the pyrolysis of BCS at 5 °C/min and different particle sizes.

Heating Rates Effect

The TGA and DTG curves obtained from the Nanche endocarp by modifying the heating rate are presented in Figure 2. The thermal degradation is divided into three stages, as shown in the corresponding figure. The DTG curves initially indicate endothermic dehydration and moisture loss in the first stage (drying stage, 30–150 °C) with a mass loss between 3.21 to 3.82%, which means that the biomass has less than 5% moisture, so it can be considered feasible for combustion. The decay in the degree of conversion during the second stage (active pyrolytic stage, 150–450 °C) is characteristic of lignocellulosic biomasses [39], and this stage has two zones, i.e., in a temperature range of 250 to 300 °C (Z_1) corresponds to the degradation of hemicellulose. Subsequently, at a temperature between 320 °C and 380 °C (Z_2) indicates the degradation of cellulose and part of lignin, and it is this stage that contributes most to mass loss (>60%). Finally, the third stage (passive pyrolytic stage, > 450 °C) corresponds to the degradation of lignin and the formation of charcoal. Yang et al. [40] report the temperature ranges for the degradation of hemicellulose, cellulose, and lignin

as 220–315, 315–400, and 160–900 °C, respectively, and more specifically, it has been found that cellulose degrades between 277 and 427 °C, hemicellulose around 197 and 327 °C and lignin between 277 and 527 °C [33].

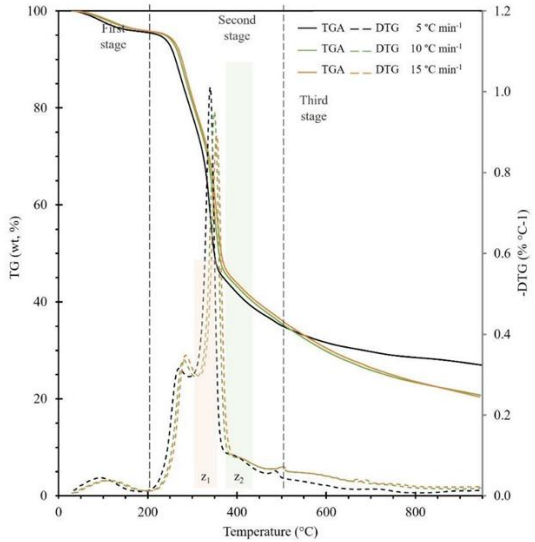

Figure 2: TGA and DTG curves for the pyrolysis of BCS at different heating rates 5, 10, and 15 °C/min and particle size D_{p4}.

Furthermore, it is observed that when the heating rate is high, the degradation rate becomes slower due to the restriction of heat transfer between the particles, as opposed to a slow heating rate where the heat remains in the biomass for a longer time, thus resulting in an intense heat transfer between the particles favoring a higher degradation rate, allowing a greater amount of dehydration, depolymerization, carbonylation, carboxylation, and transglycosylation reactions [37], thus causing a decrease in the DTG_{max} value (%/°C) presented in Table 3.

Table 3: Peak temperatures and residues of different particle sizes of BCS sample and different heating rates.

BCS sample (5 °C/min)	D_{p1}	D_{p2}	D_{p3}	D_{p4}
Particle size (μm)	75–150	150–300	600–850	850–1680
$Peak_{max.}$Temp. (°C)	338.85	336.28	341.49	340.03
DTG_{max} (%/°C)	0.7932	0.8125	1.020	1.01
$Residue_{940°C}$ (%)	21.87	20.46	26.45	27.08
BCS D_{p4} Heating rate °C/min)	5 °C/min	10 °C/min	15 °C/min	
$Peak_{max,1}$ Temp. (°C)	269.98	280.55	285.45	
$Peak_{max,2}$ Temp. (°C)	340.03	394.56	354.54	
DTG_{max} (%/°C)	1.01	0.95	0.89	
$Residue_{940°C}$ (%)	27.08	20.86	20.48	

Concerning the fact that a reverse behavior is observed in the temperature range of 315–400 °C with respect to the hemicellulose decomposition, this can be explained by the behavior of the cellulose decomposition reported by Várhegyi et al. [41], where mass transfer problems caused by high heating rates can delay the decomposition process, and in the case of cellulose the presence of reaction products during its decomposition can initiate autocatalytic reactions and cellulose can be consumed below the maximum cellulose decomposition temperatures, thus causing a shift and decrease in the maximum peak cellulose degradation of DTG's as in the present study. Finally, yields of 31.61, 29.84, and 30.45% were observed for heating rates of 5, 10, and 15 °C/min, respectively, at a temperature of 600 °C. Thus, Nanche endocarp can be considered a very good precursor for the generation of biochar and volatile compounds by slow pyrolysis [35].

Saffe et al. [42] have reported an estimation of hemicellulose, cellulose, and lignin contents of various agro-industrial wastes based on a deconvolution technique of the dα/dT vs. T profiles as observed in Figure 3. This technique is applied to clearly separate all the peaks corresponding to the degradation of the three natural polymers contained in the biomass, and their contents are determined with the size ratio of the areas under

these peaks. The deconvolution of the dα/dT vs. T curves in the present study was carried out using Origin 9.0 software. Figure 3 shows the results obtained using this technique for the heating rate of β = 5 °C/min. A Gaussian equation was used to fit each peak as described by Perejón et al. [43] where a mathematical model was proposed, and its integration allowed to estimate the percentage of hemicellulose, cellulose, and lignin content corresponding to the Nanche stone.

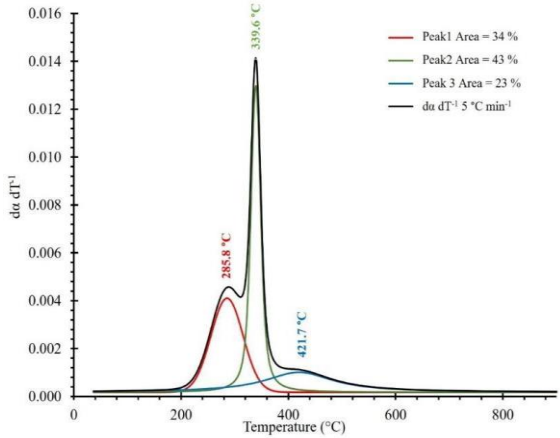

Figure 3: Deconvolution curves for the pyrolysis of BCS at 5 °C/min and particle size Dp_4.

Based on the findings depicted in Figure 3, a thorough analysis reveals distinct deconvolution results for the various components of the Nanche stone. Notably, the deconvolution of the first peak, corresponding to hemicellulose, initiates at a temperature of approximately 204 °C and concludes around 380 °C. This peak exhibits a prominent maximum at 285.8 °C, indicative of hemicellulose decomposition. Additionally, a second peak is evident, representing the cellulose component. Its deconvolution demonstrates a temperature range starting at approximately 220 °C and ending at 440 °C. The peak exhibits a maximum value at 339.6 °C, reflecting the specific characteristics of cellulose degradation.

Furthermore, a third peak emerges from the deconvolution process, beginning at around 240 °C and extending up to 700 °C. This peak exhibits a maximum value at 421.7 °C, directly associated with the lignin content present in the Nanche stone.

These deconvolution results provide valuable insights into the thermal behavior and decomposition characteristics of the Nanche stone's constituent components. By accurately identifying and analyzing these distinct peaks, a comprehensive understanding of the thermal profile and composition of the Nanche stone can be attained based on the hemicellulose, cellulose, and lignin content. Please refer to Figure 3 for a visual representation of these deconvolution outcomes.

The obtained results presented in Figure 3 align closely with the findings reported in existing literature for similar lignocellulosic biomass [44]. Through the deconvolution process, it becomes evident that the percentage of area associated with each of the three peaks corresponds remarkably well to the theoretical percentage content of hemicellulose, cellulose, and lignin, which are 34%, 43%, and 23%, respectively.

This agreement between the deconvolution results and the theoretical composition further strengthens the reliability and accuracy of the analysis. It is noteworthy to mention that these results closely align with the compositional analysis data reported in Table 2, providing a consistent and coherent characterization of the Nanche stone's constituents.

The agreement between the deconvolution findings, theoretical percentages, and the compositional analysis outcomes underscores the robustness and validity of the experimental methodology employed. Such a convergence of results reinforces the confidence in the obtained data and supports our understanding of the composition and thermal behavior of the Nanche stone.

It is essential to acknowledge the significance of these results as they contribute to the growing body of knowledge regarding

lignocellulosic biomass and offer valuable insights for further research and practical applications.

Kinetic Triplet Analysis

Apparent Activation Energy

Figure 4a-c shows the linear fit plots obtained using the KAS, FWO, and SK isoconversional methods for determining the apparent activation energy. It is observed that the isoconversional lines generated by these methods exhibit parallel behavior within a specific range of conversion (α) from 0.1 to 0.65. However, for higher conversion degrees ($\alpha \geq 0.7$), slight deviations are observed, indicating that reactions beyond this threshold become more complex.

The parallel nature of the isoconversional lines within the range of 0.1 to 0.65 suggests a consistent activation energy throughout this region, indicating a relatively uniform reaction mechanism. However, the emergence of deviations beyond $\alpha \geq 0.7$ implies a deviation from this uniform behavior, suggesting the involvement of additional factors or mechanisms influencing the reaction kinetics.

These findings shed light on the complexity of the reactions occurring beyond $\alpha \geq 0.7$, indicating the presence of additional factors that contribute to the reaction pathway. It is crucial to consider these deviations and the associated complexity when analyzing and interpreting the kinetics of the reactions at higher conversion degrees [6]. For a visual representation of these results, please refer to Figure 4a-c.

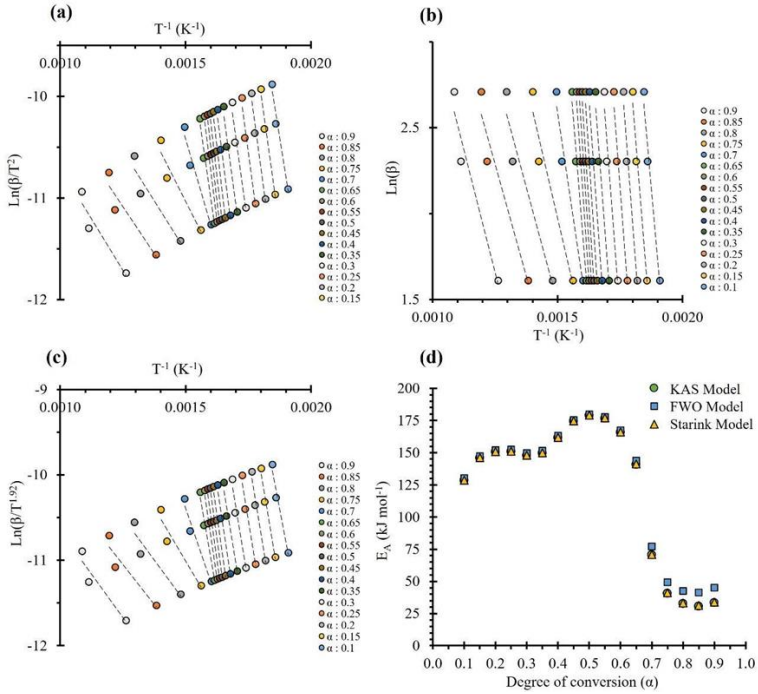

Figure 4: Linear plots of (a) KAS; (b) FWO model; (c) SK model: and (d) EA depending on the degree of conversion

Figure 4d illustrates the apparent activation energy derived from various isoconversional methods. Notably, the KAS, FWO, and SK methods exhibit a distinct range wherein the apparent activation energy reaches its maximum value at approximately α = 0.5 (334.4–352.2 °C). This range corresponds to the second phase of the active pyrolytic stage, specifically the region wherein cellulose degradation peaks according to the DTG diagram presented in Figure 2. The observed phenomenon can be attributed to the increased energy requirement for the degradation of cellulose present in the biomass. Additionally, as the degree of conversion advances from 0.5 to 0.85, it was observed that the apparent activation energy diminishes. This observation suggests that the pyrolysis of BCS involves a complex series of reactions, resulting in a minimal presence of cellulose and hemicellulose beyond a conversion degree of α > 0.5 [20]. Consequently, this decrease in apparent activation

energy occurs. The average values of the calculated apparent activation energy were determined to be 122.3 kJ/mol (KAS), 126.3 kJ/mol (FWO), and 122.7 kJ/mol (SK), as indicated in Table 4. Following the recommendations of ICTAC, the Starink method was selected as the most suitable model for representing the apparent activation energy in BCS pyrolysis. The results obtained from the SK model demonstrated excellent agreement, with a deviation of less than 6%. This outcome not only validates the accuracy of the calculations but also confirms the predictive capability of the SK method. Therefore, the data derived from the SK model was employed for subsequent calculations in the present study.

Table 4: Apparent activation energy (EA) of pyrolysis of BCS determined by isoconversional methods.

	KAS		FWO		SK	
α	E_A (kJ/mol)	R^2	E_A (kJ/mol)	R^2	E_A (kJ/mol)	R^2
0.10	128.3	0.98	130.4	0.98	128.6	0.98
0.15	145.8	0.98	147.3	0.98	146.1	0.98
0.20	150.6	0.97	151.9	0.97	150.8	0.97
0.25	150.8	0.96	152.4	0.97	151.1	0.96
0.30	147.9	0.96	149.8	0.96	148.1	0.96
0.35	149.6	0.96	151.6	0.96	149.9	0.96
0.40	161.7	0.97	163.2	0.97	161.9	0.97
0.45	174.4	0.98	175.4	0.98	174.6	0.98
0.50	178.9	0.98	179.8	0.99	179.2	0.98
0.55	176.7	0.99	177.8	0.99	177.0	0.99
0.60	165.9	0.99	167.5	0.99	166.1	0.99
0.65	140.9	0.98	143.9	0.98	141.2	0.98
0.70	70.6	0.96	77.3	0.97	70.9	0.96
0.75	40.8	0.92	49.4	0.95	41.2	0.92
0.80	32.8	0.89	42.6	0.94	33.3	0.89
0.85	30.7	0.88	41.5	0.94	31.2	0.88
0.90	33.4	0.90	45.2	0.95	34.0	0.90
Average	122.3	0.95	126.3	0.97	122.7	0.96

The apparent activation energy represents the minimum energy required for a reaction to occur. Therefore, higher values of apparent activation energy indicate greater difficulty in initiating the pyrolysis reactions. In a study by El May et al. [45] focusing on date stone, a relatively low apparent activation energy of 58.9 kJ/mol was calculated. It is important to note that date stone possesses a different composition and characteristics compared to Nanche stone studied in the present research (BCS). However, when comparing the apparent activation energy of the current study with other stones exhibiting similar characteristics, such as olive and plum stones, the differences observed are relatively minor. Garcia et al. [46] conducted a study on olive stone pyrolysis and reported an apparent activation energy value of 198.7 kJ/mol. In a separate investigation by Ceylan [44] focusing on plum stone pyrolysis, an apparent activation energy of 154.8 kJ/mol was obtained. Damartzis et al. [47] examined the pyrolysis kinetics of cardoon (*Cynara cardunculus*) and determined an apparent activation energy of 223.8 kJ/mol. Amutio et al. [48] investigated the pyrolysis of pine wood residues and observed a range of apparent activation energy values from 63 to 205.8 kJ/mol. Overall, the apparent activation energy values calculated for Nanche stone exhibit similarities to those reported in previous studies on biomass residues. It is essential to emphasize that the apparent activation energy values obtained for different degrees of conversion should not be regarded as the definitive values for specific reaction steps. Instead, they represent apparent values that encompass the contributions of various parallel and competing reactions, influencing the overall reaction rate [15,19].

Table 5 presents the apparent activation energy values obtained using the FWO model for different biomasses, including information on their structural composition and elemental ratios. Additionally, one of the crucial thermal parameters for biomass and waste solid fuels, namely the higher heating value (HHV), is included. The HHV represents the maximum energy content that can potentially be recovered from solid fuels [49, 50].

Table 5: Comparison of apparent activation energy, structural composition, elemental ratios, and HHV values by different biomass.

Sample	**E_A (kJ/mol)**	**HE [a] (%)**	**CE [b] (%)**	**LI [c] (%)**	**O/C Ratio**	**H/C Ratio**	**HHV [d] (MJ/kg)**	**Reference**
BCS	122.7 [e]	21.17	44.16	34.67	0.861	0.113	17.92	This study
Avocado stone	88.9 [f]	76.4	3.0	17.0	1.021	0.138	17.24	Sangaré et al. [6]
Agave salmiana bagasse	111.6 [f]	43.8	40.7	14.2	1.507	0.107	9.65	
Cocoa Shell	197.7 [f]	45.4	7.8	21.5	0.678	0.132	21.06	
α-Cellulose	166.4 [f]	-	100	-	1.258	0.157	15.10	
Apple pomace	194.8 [f]	27.77	47.49	24.72	0.780	0.138	19.66	Baray-Guerrero et al. [19]
Azadirachta indica	193.7 [f]	24.64	38.61	12.89	0.750	0.144	20.83	Mishra et al. [5]
Phyllanthus emblica kernel	195.1 [f]	21.43	46.11	10.22	0.803	0.137	20.08	
Garlic husk	154.9 [f]	29.34	41.32	17.14	1.255	0.109	12.46	Singh et al. [20]
Acacia nilótica	221.6 [f]	28.64	41.66	24.20	1.105	0.172	17.86	Singh et al. [4]
Banana leaves	84 [f]	34.34	43.34	15	1.116	0.157	17.80	Singh et al. [51]

[a] Hemicellulose, [b] Cellulose, [c] Lignin, [d] Higher heating value calculated by Demirbaş formula [52], [e] Calculated by Starink model. [f] Calculated by FWO model.

The values presented in Table 5 clearly show that cellulose has a high apparent activation energy (166.42 kJ/mol). However, it has a relatively intermediate higher heating value (15.10 MJ/kg). On the other hand, cocoa husk has the highest HHV value (21.06 MJ/kg), which can be correlated with the elemental components of the biomass as demonstrated by the Van-Krevelen diagram in Figure 5. Notably, all the analyzed biomasses differ in their O/C and H/C ratios. When the O/C ratio is plotted against the HHV value, it is evident that biomasses having a small O/C ratio value have the highest HHV value. It is also well-known that there is a strong correlation between the apparent activation energy and lignin content, which governs the structural composition of biomass.

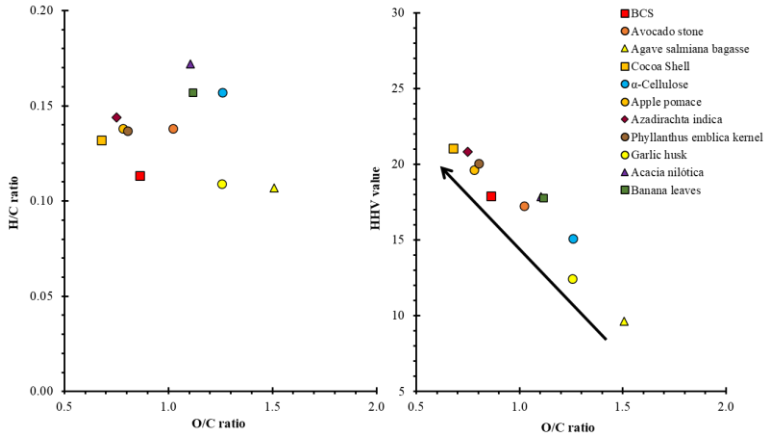

Figure 5: (a) Van-Krevelen plot and (b) Correlation O/C ratio vs. HHV value of biomasses.

A high apparent activation energy in biomass does not necessarily confer benefits, as it indicates that not all the energy utilized during the pyrolysis process for thermal degradation of the biomass will be effectively converted into valuable solid, liquid, and gaseous products. For instance, the cocoa shell contains a substantial amount of hemicellulose, which consists of organic matter characterized by relatively weak energetic bonds resulting from its structural arrangement. Consequently, the thermal degradation of hemicellulose is expected to yield simpler combustible products (both liquid and gaseous) compared to

biomass with higher cellulose and lignin content [50]. Therefore, a higher apparent activation energy may not always result in the efficient generation of energetically valuable byproducts during biomass pyrolysis. A clarifying example can be observed with apple pomace and *Phyllanthus emblica* kernel, both of which exhibit higher cellulose and lignin content. This composition results in a higher higher heating value (HHV) accompanied by a moderate increase in the apparent activation energy. In the case of BCS endocarp, a similar energy balance is observed. It possesses a substantial amount of cellulose, along with moderate quantities of hemicellulose and lignin. This composition contributes to a relatively high HHV value (17.92 MJ/kg) accompanied by a comparatively lower average apparent activation energy (122.7 kJ/mol) when compared to other biomasses listed in Table 5. These characteristics make BCS endocarp highly suitable for utilization in pyrolytic processes aimed at generating value-added energy.

Pre-Exponential Factor (A_α)

The pre-exponential factor values were determined using the Kissinger method, utilizing the apparent activation energies obtained from the SK method. The pre-exponential factor holds significant importance as it is a crucial parameter in pyrolysis, playing a fundamental role in the design and optimization of pyrolysis reactors [18,53]. By employing Equation (12), the values of Aα corresponding to the degree of conversion at a heating rate of 15 °C/min were calculated and are presented in Table 6. The values of A_α associated with the pyrolysis of BCS exhibited a range of variations from 105 to 1014 min^{-1} as the degree of conversion increased from 0.1 to 0.7. This range corresponds to the phase of highest pyrolytic activity, primarily driven by the degradation of hemicellulose and cellulose. It is suggested that the reactions occurring during this range of conversion are complex and demand higher energy input to proceed [54]. However, when the degree of conversion reaches the range of 0.75 to 0.9, the pre-exponential factor experiences a decrease in its value, falling within the range of 101 to 102 min^{-1}. This decrease indicates that the biomass conversion has

entered the passive pyrolytic stage, where less energy is required to sustain the pyrolysis process.

Table 6: Apparent activation energy (E_A) by the Starink model, pre-exponential factor (A_α) by the Kissinger method, and thermodynamics properties for pyrolysis of BCS.

α	**E_A (kJ/mol)**	**A_α (min^{-1})**	**Gibbs Free Energy ΔG (kJ/mol):**	**Enthalpy ΔH (kJ/mol):**	**Entropy ΔS (kJ/mol):**
0.10	128.6	2.9×10^{10}	181.8	123.3	−93.1
0.15	146.1	9.6×10^{11}	181.1	140.9	−64.1
0.20	150.8	2.5×10^{12}	180.9	145.6	−56.3
0.25	151.1	2.6×10^{12}	180.9	145.9	−55.9
0.30	148.1	1.4×10^{12}	181.0	142.9	−60.7
0.35	149.9	2.1×10^{12}	181.0	144.7	−57.8
0.40	161.9	2.2×10^{13}	180.6	156.7	−38.0
0.45	174.6	2.7×10^{14}	180.2	169.4	−17.1
0.50	179.2	6.7×10^{14}	180.0	174.0	−9.6
0.55	177.0	4.3×10^{14}	180.1	171.7	−13.3
0.60	166.1	5.1×10^{13}	180.4	160.9	−31.1
0.65	141.2	3.6×10^{11}	181.3	136.0	−72.2
0.70	70.9	2.6×10^{5}	184.9	65.7	−189.8
0.75	41.2	5.1×10^{2}	187.7	36.0	−241.7
0.80	33.3	9.0×10^{1}	188.8	28.1	−256.1
0.85	31.2	5.7×10^{1}	189.1	26.0	−259.9
0.90	34.0	1.0×10^{2}	188.7	28.8	−254.8
Average	122.7	8.6×10^{13}	182.8	117.4	−104.2

Reaction Model f(α)

The master plot method was employed to determine the most probable reaction model during the pyrolysis of BCS. Figure 6a displays all the theoretical models described in Table 2 alongside the experimental curve. The master plots were calculated using Equation (14) within the range of 0.1 to 0.9, while the experimental data were generated using a heating rate of 15 °C/min and the apparent activation energy determined by the SK method.

As depicted in Figure 6a, the experimental curves were fitted to three reaction models as a function of the degree of conversion. For a heating rate of 15 °C/min, it was found that a seventh-order reaction model, $f(\alpha) = (1 - \alpha)^7$, with a sum of squared errors

(SSE) of 0.0004, best describes the pyrolysis process when $\alpha \leq 0.25$. In the range of $0.3 \leq \alpha \leq 0.45$, a fourth-order model, $f(\alpha) = (1 - \alpha)^4$, was observed to be the most suitable, yielding an SSE of 0.0103. Furthermore, for $0.5 \leq \alpha \leq 0.7$, the best fit was achieved with a second-order model of 2.48, $f(\alpha) = (1 - \alpha)^{2.48}$, resulting in an SSE of 0.0056 (Figure 6b).

It is clear from the results that the order of the reaction decreases with an increasing degree of conversion. This trend can be attributed to the growing probability of molecular collision as the temperature rises, leading to a higher decomposition rate of hemicellulose and cellulose. Consequently, the reaction order decreases from 7 to 2.48. It is worth noting that the presence of lignin in BCS contributes to its complex and rigid cross-linked phenolic structure.

When the degree of conversion reaches $\alpha \geq 0.75$, the reaction model becomes a result of the combined effects of various mechanisms such as nucleation, diffusion, and power effects [18]. This observation aligns with the isoconversion lines displayed in Figure 4, where the deviation from a single reaction model correlates with the occurrence of complex reactions [6]. It is worth emphasizing that a high reaction order indicates a low probability of molecular collision, which has been observed in other biomass materials like bamboo waste and cocoa shell [18,55]. Therefore, considering the compositional characteristics of the biomass studied, the presence of high lignin content implies a complex and rigid cross-linked phenolic structure. Consequently, pyrolysis at lower degrees of conversion involves the combined effects of various mechanisms, including nucleation, diffusion, and power effects. Hence, the elevated reaction order observed in this study may arise from the combined influence of these mechanisms [56].

Once the kinetic triplets of BCS pyrolysis are estimated, it becomes possible to construct a kinetic expression using Equation (5). The averages of the SK apparent activation energy and pre-exponential factors corresponding to the appropriate range of conversion degrees are incorporated into the following equations:

$$\frac{d\alpha}{dT} = \begin{cases} 1.5x10^{12} exp\left(\frac{-17335.1}{T}\right)(1-\alpha)^{7}, \alpha \leq 0.25\ (264.4-302.8\ ℃) \\ 7.5x10^{13} exp\left(\frac{-19082.2}{T}\right)(1-\alpha)^{4}, 0.3 \leq \alpha \leq 0.45\ (316.2-343\ ℃) \\ 2.3x10^{14}\ exp\left(\frac{-17665.7}{T}\right)(1-\alpha)^{2.48}, 0.5 \leq \alpha \leq 0.7\ (347.5-385.6\ ℃) \end{cases} \quad (19)$$

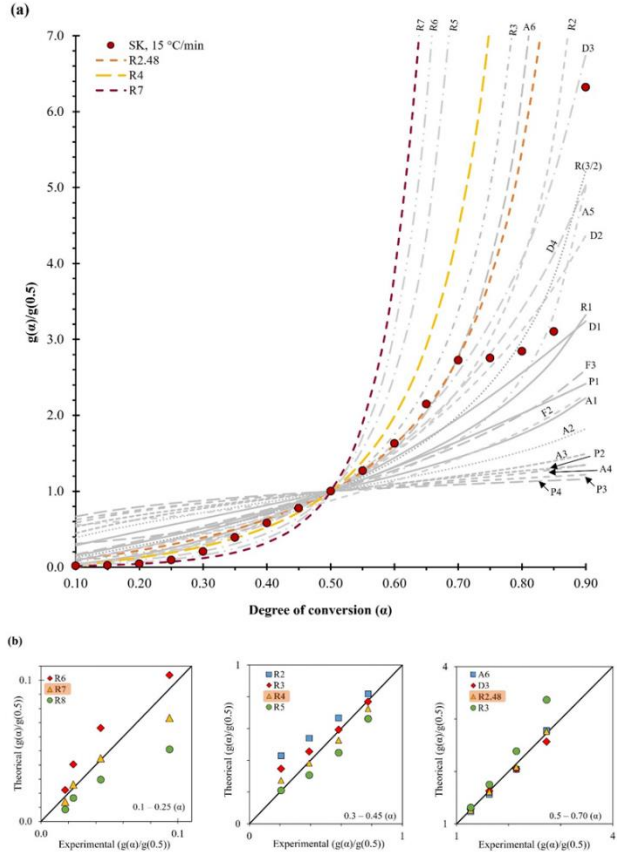

Figure 6: (**a**) Reaction models using generalized master plot method (g(α)/g(0.5) vs. α), and (**b**) experimental and theoretical curves (g(α)/g(0.5)).

Thermodynamics Analysis

The thermodynamic parameters, enthalpy, Gibbs free energy, and entropy were plotted as a function of the degree of conversion (α) (Figure 7), and the numerical values are shown in Table 6. All these calculations were conducted using the apparent activation energy determined through the SK method and the pre-exponential factor obtained from the Kissinger

method at a heating rate of 15 °C/min. The assessment of thermodynamic properties is crucial in defining the operational conditions of a process. In this regard, ΔH is defined as the energy consumed during the conversion of biomass into various pyrolytic products. The average value obtained for ΔH was 117.4 kJ/mol. Furthermore, the disparity between E_A and ΔH represents the energy difference between the reactant and the activated complex and termed the "potential energy barrier," as it provides insights into the ease of activated complex formation. In this study, the value of this potential energy barrier was found to be 5.2 kJ/mol, which is less than the threshold of 5.5 kJ/mol. This value of 5.2 kJ/mol found in the study suggests that the pyrolysis of BCS is a feasible reaction to produce bioenergy, as little additional energy is required to achieve product generation. This result is consistent with previous studies by Mumbach et al. and Sangaré et al. [18,22]. These findings suggest that the formation of activated complexes is favorable [18,57], and the pyrolysis reaction can proceed with ease. In other words, pyrolysis can be carried out by providing only a minimal amount of additional energy [6].

The analysis and understanding of these values are crucial for the design of a pyrolysis reactor, as it entails ensuring sufficient heat transfer to supply the required energy for biomass conversion [58]. The Gibbs free energy serves as a measure of the overall energy change during a reaction in a thermal process and offers valuable insights into the spontaneity and direction of reactions. A positive value of ΔG indicates non-spontaneity, while a significantly large value suggests a lower feasibility of the reaction [56]. The average value of ΔG was determined to be 182.8 kJ/mol, with a maximum deviation of ± 3.5 kJ/mol. The positive value of ΔG indicates that the pyrolysis reaction of BCS is non-spontaneous, highlighting the need for additional energy for the conversion of biomass into different pyrolytic products. On the other hand, ΔS values are employed to qualitatively assess the reactivity of the system [59]. In this study, an average ΔS value of -104.2 J/mol·K was obtained, providing insights into the system's reactivity. The negative value of ΔS indicates that the reactions are nearing thermodynamic equilibrium and exhibit higher thermodynamic reversibility. Consequently, the degree of disorder in the products is lower than that in the reactants [6,18].

This behavior is particularly evident at a conversion close to α = 0.5, which agrees with the peak observed in the DTG curves corresponding to cellulose, a highly reactive component during pyrolysis [6,50]. Furthermore, the average apparent activation energy values obtained from this biomass highlight its potential as a greatly desirable energy source for bioenergy applications.

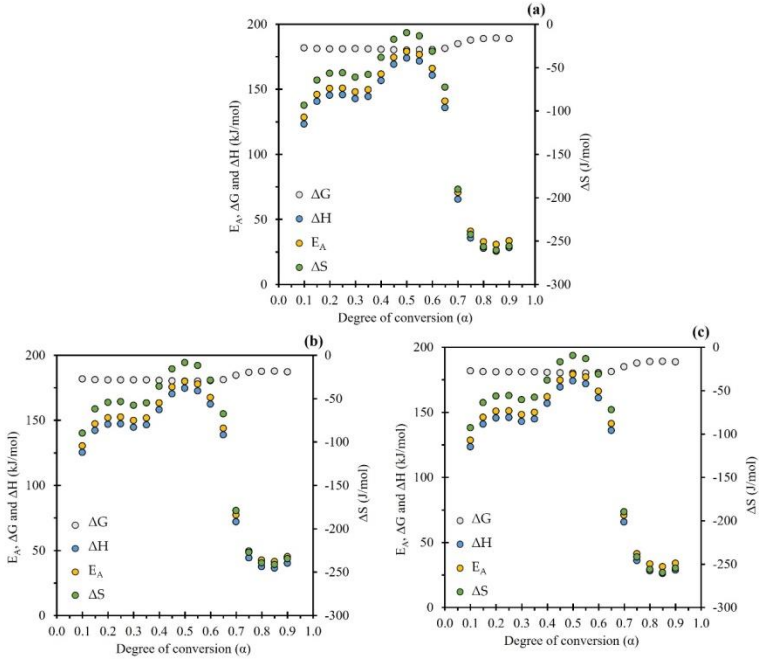

Figure 7: Thermodynamic parameters from the (**a**) KAS, (**b**) FWO, and (**c**) Starink methods.

Conclusions

This study presented the first investigation of the pyrolysis kinetics of Nanche stone (BCS) using thermogravimetric analysis. The favorable characteristics of BCS, including its low moisture and ash content, along with a high volatile matter content (≥70%), position it as a promising candidate to produce diverse bioenergy products.

The average apparent activation energies obtained from different methods (KAS, FWO, and SK) were found to be quite similar, averaging around 123.8 kJ/mol. Additionally, the evaluation of

the pre-exponential factor as a function of the degree of conversion using the Kissinger method showed a wide range from 105 to 1014 min^{-1} during the stage of highest pyrolytic activity. These findings indicate that the BCS system is highly reactive to temperature and suggest that the n-order reaction models best describe the pyrolysis process.

Furthermore, the thermodynamic analysis revealed a small difference between the apparent activation energy (E_A) and the enthalpy change (ΔH), with a value of 5.2 kJ/mol. This close proximity between E_A and ΔH favors the pyrolysis reaction and indicates the feasibility of the energetic process.

It is worth emphasizing that the complex and rigid cross-linked structure of BCS, attributed to its high lignin and cellulose content, plays a significant role in its pyrolysis behavior. The kinetic triplet analysis, involving the apparent activation energy, pre-exponential factor, and reaction model, indicated that the pyrolysis pattern of this biomass closely aligns with high-order reaction kinetics. This behavior can be attributed to the combined influence of diffusion and power law models.

Importantly, this study represents the first investigation into the pyrolysis kinetics of Nanche (*Byrsonima crassifolia*) stone as a biomass waste. The findings derived from the kinetics triplets and thermodynamic parameters highlight the great potential of this biomass as a valuable bioenergy resource. These results underscore the feasibility of utilizing BCS for bioenergy applications, thus contributing to the sustainable utilization of this biomass waste.

References

1. Luo L, Guo X, Zhang Z, Chai M, Rahman MdM, et al. Insight into Pyrolysis Kinetics of Lignocellulosic Biomass: Isoconversional Kinetic Analysis by the Modified Friedman Method. Energy & Fuels. 2020; 34: 4874–4881.
2. Missaoui A, Bostyn S, Belandria V, Cagnon B, Sarh B, et al. Hydrothermal Carbonization of Dried Olive Pomace: Energy Potential and Process Performances. J Anal Appl Pyrolysis. 2017; 128: 281–290.

3. Pravin Kumar SA, Nagarajan R, Midhun Prasad K, Anand B, Murugavelh S. Thermogravimetric Study and Kinetics of Banana Peel Pyrolysis: A Comparison of 'Model-Free' Methods. Biofuels. 2022; 13: 129–138.
4. Singh S, Prasad Chakraborty J, Kumar Mondal M. Intrinsic Kinetics, Thermodynamic Parameters and Reaction Mechanism of Non-Isothermal Degradation of Torrefied Acacia Nilotica Using Isoconversional Methods. Fuel. 2020; 259: 116263.
5. Mishra RK, Mohanty K. Characterization of Non-Edible Lignocellulosic Biomass in Terms of Their Candidacy towards Alternative Renewable Fuels. Biomass Convers Biorefin. 2018; 8: 799–812.
6. Sangaré D, Bostyn S, Moscosa Santillán M, García-Alamilla P, Belandria V, et al. Comparative Pyrolysis Studies of Lignocellulosic Biomasses: Online Gas Quantification, Kinetics Triplets, and Thermodynamic Parameters of the Process. Bioresour Technol. 2022; 346: 126598.
7. Agredano-De la Garza CS, Balois-Morales R, Berumen-Varela G, León-Fernández AE, Bautista-Rosales PU, et al. Physicochemical Characterization and Dietary Fiber of 15 Nance (Byrsonima Crassifolia L.) Fruits Selections from Nayarit. Sci Hortic. 2021; 289: 110460.
8. Espinosa-Rodríguez MÁ, Hidalgo-Millán A, Delgado-Delgado R, Olvera-Izaguirre L, Bernal-Jácome LA. Adsorción de Cd(II) y Pb(II) Presentes En Solución Acuosa Con Hueso de Nanche (Byrsonima Crassifolia). Revista Colombiana de Química. 2020; 48: 30–36.
9. Claudia M Rezende, Sandra RG Fraga. Chemical and Aroma Determination of the Pulp and Seeds of Murici (Byrsonima Crassifolia L.). J Braz Chem Soc. 2003; 14.
10. de Souza VR, Pereira PAP, Queiroz F, Borges SV, de Deus Souza Carneiro J. Determination of Bioactive Compounds, Antioxidant Activity and Chemical Composition of Cerrado Brazilian Fruits. Food Chem. 2012; 134: 381–386.
11. Servicio de Información Agroalimentaria y Pesquera Sistema de Información Agroalimentaria de Consulta.
12. Caballero-Roque A, Gilber V, Pérez J, Escobar R, Ballinas J. Uso de Nanche (Byrsonima Crassifolia (L.) Kunth) En Gelatina Artesanal Para Niños. Etnobiología. 2012; 10: 50–

55.
13. Alves JLF, da Silva JCG, da Silva Filho VF, Alves RF, Ahmad MS, et al. Bioenergy Potential of Red Macroalgae Gelidium Floridanum by Pyrolysis: Evaluation of Kinetic Triplet and Thermodynamics Parameters. Bioresour Technol. 2019; 291: 121892.
14. Ferreira MFP, Oliveira BFH, Pinheiro WBS, Correa NF, França LF, et al. Generation of Biofuels by Slow Pyrolysis of Palm Empty Fruit Bunches: Optimization of Process Variables and Characterization of Physical-Chemical Products. Biomass Bioenergy. 2020; 140: 105707.
15. Cai J, Xu D, Dong Z, Yu X, Yang Y, et al. Processing Thermogravimetric Analysis Data for Isoconversional Kinetic Analysis of Lignocellulosic Biomass Pyrolysis: Case Study of Corn Stalk. Renewable and Sustainable Energy Reviews. 2018; 82: 2705–2715.
16. Rasool T, Najar I, Srivastava VC, Pandey A. Pyrolysis of Almond (Prunus Amygdalus) Shells: Kinetic Analysis, Modelling, Energy Assessment and Technical Feasibility Studies. Bioresour Technol. 2021; 337: 125466.
17. Açıkalın K. Determination of Kinetic Triplet, Thermal Degradation Behaviour and Thermodynamic Properties for Pyrolysis of a Lignocellulosic Biomass. Bioresour Technol. 2021; 337: 125438.
18. Mumbach GD, Alves JLF, da Silva JCG, di Domenico M, de Sena RF, et al. Pyrolysis of Cocoa Shell and Its Bioenergy Potential: Evaluating the Kinetic Triplet, Thermodynamic Parameters, and Evolved Gas Analysis Using TGA-FTIR. Biomass Convers Biorefin. 2022; 12: 723–739.
19. Guerrero MRB, Marques Da Silva Paula M, Zaragoza MM, Gutiérrez JS, Velderrain VG, et al. Thermogravimetric Study on the Pyrolysis Kinetics of Apple Pomace as Waste Biomass. Int J Hydrogen Energy. 2014; 39: 16619–16627.
20. Singh RK, Patil T, Sawarkar AN. Pyrolysis of Garlic Husk Biomass: Physico-Chemical Characterization, Thermodynamic and Kinetic Analyses. Bioresour Technol Rep. 2020; 12: 100558.
21. Mani T, Murugan P, Abedi J, Mahinpey N. Pyrolysis of Wheat Straw in a Thermogravimetric Analyzer: Effect of Particle Size and Heating Rate on Devolatilization and

Estimation of Global Kinetics. Chemical Engineering Research and Design. 2010; 88: 952–958.
22. Sangare D, Chartier A, Moscosa-Santillan M, Gökalp I, Bostyn S. Kinetic Studies of Hydrothermal Carbonization of Avocado Stone and Analysis of the Polycyclic Aromatic Hydrocarbon Contents in the Hydrochars Produced. Fuel. 2022; 316: 123163.
23. Friedman HL. Kinetics of Thermal Degradation of Char-Forming Plastics from Thermogravimetry. Application to a Phenolic Plastic. Journal of Polymer Science Part C: Polymer Symposia. 1964; 6: 183–195.
24. Muravyev N, Vyazovkin S. The Status of Pyrolysis Kinetics Studies by Thermal Analysis: Quality Is Not as Good as It Should and Can Readily Be. Thermo. 2022; 2: 435–452.
25. Vyazovkin S, Burnham AK, Criado JM, Pérez-Maqueda LA, Popescu C, et al. ICTAC Kinetics Committee Recommendations for Performing Kinetic Computations on Thermal Analysis Data. Thermochim Acta. 2011; 520.
26. Koga N, Vyazovkin S, Burnham AK, Favergeon L, Muravyev Nv, et al. ICTAC Kinetics Committee Recommendations for Analysis of Thermal Decomposition Kinetics. Thermochim Acta. 2023; 719: 179384.
27. White JE, Catallo WJ, Legendre BL. Biomass Pyrolysis Kinetics: A Comparative Critical Review with Relevant Agricultural Residue Case Studies. J Anal Appl Pyrolysis. 2011; 91: 1–33.
28. Kumar M, Upadhyay SN, Mishra PK. A Comparative Study of Thermochemical Characteristics of Lignocellulosic Biomasses. Bioresour Technol Rep. 2019; 8: 100186.
29. Kissinger HE. Reaction Kinetics in Differential Thermal Analysis. Anal Chem. 1957; 29: 1702–1706.
30. Akahira T, Sunuse TT. Joint Convention of Four Electrical Institutes. Research Report, Chiba Institute of Technology, Chiba. 1971; 16: 22–31.
31. Ozawa T. A New Method of Analyzing Thermogravimetric Data. Bull Chem Soc Jpn. 1965; 38: 1881–1886.
32. Flynn JH, Wall LA. A Quick, Direct Method for the Determination of Activation Energy from Thermogravimetric Data. J Polym Sci B. 1966; 4: 323–328.
33. Du Z, Sarofim AF, Longwell JP. Activation Energy

Distribution in Temperature-Programmed Desorption: Modeling and Application to the Soot Oxygen System. Energy & Fuels. 1990; 4: 296–302.
34. Starink MJ. The Determination of Activation Energy from Linear Heating Rate Experiments: A Comparison of the Accuracy of Isoconversion Methods. Thermochim Acta. 2003; 404: 163–176.
35. Kumi AG, Ibrahim MG, Nasr M, Fujii M. Biochar Synthesis for Industrial Wastewater Treatment: A Critical Review. Materials Science Forum. 2020; 1008: 202–212.
36. Shimada N, Kawamoto H, Saka S. Different Action of Alkali/Alkaline Earth Metal Chlorides on Cellulose Pyrolysis. J Anal Appl Pyrolysis. 2008; 81: 80–87.
37. Dwivedi KK, Prabhansu, Karmakar MK, Chatterjee PK. Thermal Degradation, Characterization and Kinetic Modeling of Different Particle Size Coal through TGA. Thermal Science and Engineering Progress. 2020; 18: 100523.
38. Luo M, Stanmore B. The Combustion Characteristics of Char from Pulverized Bagasse. Fuel. 1992; 71: 1074–1076.
39. Gašparovič L, Koreňová Z, Jelemenský Ľ. Kinetic Study of Wood Chips Decomposition by TGA. 2010; 64: 174–181.
40. Yang H, Yan R, Chen H, Lee DH, Zheng C. Characteristics of Hemicellulose, Cellulose and Lignin Pyrolysis. Fuel. 2007; 86: 1781–1788.
41. Várhegyi G, Szabó P, Antal MJ. Kinetics of the Thermal Decomposition of Cellulose under the Experimental Conditions of Thermal Analysis. Theoretical Extrapolations to High Heating Rates. Biomass Bioenergy. 1994; 7: 69–74.
42. Saffe A, Fernandez A, Mazza G, Rodriguez R. Prediction of Regional Agro-Industrial Wastes Characteristics by Thermogravimetric Analysis to Obtain Bioenergy Using Thermal Process. Energy Exploration & Exploitation. 2018; 37: 544–557.
43. Perejón A, Sánchez-Jiménez PE, Criado JM, Pérez-Maqueda LA. Kinetic Analysis of Complex Solid-State Reactions. A New Deconvolution Procedure. J Phys Chem B. 2011; 115: 1780–1791.
44. Ceylan S. Kinetic Analysis on the Non-Isothermal Degradation of Plum Stone Waste by Thermogravimetric

Analysis and Integral Master-Plots Method. Waste Management & Research. 2015; 33: 345–352.
45. el may Y, Jeguirim M, Dorge S, Trouvé G, Said R. Study on the Thermal Behavior of Different Date Palm Residues: Characterization and Devolatilization Kinetics under Inert and Oxidative Atmospheres. Energy. 2012; 44: 702–709.
46. García GB, Calero De Hoces M, Martínez García C, Cotes Palomino MT, Gálvez AR, et al. Characterization and Modeling of Pyrolysis of the Two-Phase Olive Mill Solid Waste. Fuel Processing Technology. 2014; 126: 104–111.
47. Damartzis T, Vamvuka D, Sfakiotakis S, Zabaniotou A. Thermal Degradation Studies and Kinetic Modeling of Cardoon (Cynara Cardunculus) Pyrolysis Using Thermogravimetric Analysis (TGA). Bioresour Technol. 2011; 102: 6230–6238.
48. Amutio M, Lopez G, Aguado R, Artetxe M, Bilbao J, et al. Kinetic Study of Lignocellulosic Biomass Oxidative Pyrolysis. Fuel. 2012; 95: 305–311.
49. Khunphakdee P, Korkerd K, Soanuch C, Chalermsinsuwan B. Data-Driven Correlations of Higher Heating Value for Biomass, Waste and Their Combination Based on Their Elemental Compositions. Energy Reports. 2022; 8: 36–42.
50. Huang YF, Kuan WH, Chiueh PT, Lo SL. Pyrolysis of Biomass by Thermal Analysis–Mass Spectrometry (TA–MS). Bioresour Technol. 2011; 102: 3527–3534.
51. Singh RK, Pandey D, Patil T, Sawarkar AN. Pyrolysis of Banana Leaves Biomass: Physico-Chemical Characterization, Thermal Decomposition Behavior, Kinetic and Thermodynamic Analyses. Bioresour Technol. 2020; 310: 123464.
52. Demirbaş A. Calculation of Higher Heating Values of Biomass Fuels. Fuel. 1997; 76: 431–434.
53. Vlaev L, Georgieva V, Tavlieva M. On the Kinetic Mechanism of Non-Isothermal Degradation of Solids. In Reactions and Mechanisms in Thermal Analysis of Advanced Materials. 2015; 547–578.
54. He Y, Qu Y, Liu Q, Li P, Fang S, et al. Characterization of Cornstalk and Bituminous Coal Based on Kinetic and Thermodynamic Parameter for Co-Pyrolysis. IOP Conf Ser Earth Environ Sci. 2020; 555: 012001.

55. Chen C, Miao W, Zhou C, Wu H. Thermogravimetric Pyrolysis Kinetics of Bamboo Waste via Asymmetric Double Sigmoidal (Asym2sig) Function Deconvolution. Bioresour Technol. 2017; 225: 48–57.
56. Chen D, Zhou J, Zhang Q. Effects of Heating Rate on Slow Pyrolysis Behavior, Kinetic Parameters and Products Properties of Moso Bamboo. Bioresour Technol. 2014; 169: 313–319.
57. Saha D, Sinha A, Pattanayak S, Roy B. Pyrolysis Kinetics and Thermodynamic Parameters of Plastic Grocery Bag Based on Thermogravimetric Data Using Iso-Conversional Methods. International Journal of Environmental Science and Technology. 2022; 19: 391–406.
58. Daugaard DE, Brown RC. Enthalpy for Pyrolysis for Several Types of Biomass. Energy & Fuels. 2003; 17: 934–939.